

# Muscle metabolism and activation heterogeneity by combined $^{31}\text{P}$ chemical shift and $T_2$ imaging, and pulmonary $\text{O}_2$ uptake during incremental knee-extensor exercise

Daniel T. Cannon,<sup>1,2</sup> Franklyn A. Howe,<sup>3,5</sup> Brian J. Whipp,<sup>4,6†</sup> Susan A. Ward,<sup>6,7</sup> Dominick J. McIntyre,<sup>3,8</sup> Christophe Ladroue,<sup>3,9</sup> John R. Griffiths,<sup>3,8</sup> Graham J. Kemp,<sup>10</sup> and Harry B. Rossiter<sup>1,2,4</sup>

<sup>1</sup>Rehabilitation Clinical Trials Center, Division of Respiratory & Critical Care Physiology & Medicine, Los Angeles Biomedical Research Institute at Harbor-UCLA Medical Center, Torrance, California; <sup>2</sup>School of Biomedical Sciences, University of Leeds, Leeds, United Kingdom; <sup>3</sup>Department of Biochemistry, St George's, University of London, London, United Kingdom; <sup>4</sup>Department of Physiology, St George's, University of London, London, United Kingdom; <sup>5</sup>Division of Clinical Sciences, St George's, University of London, London, United Kingdom; <sup>6</sup>Human Bio-Energetics Research Centre, Crickhowell, Powys, United Kingdom; <sup>7</sup>Centre for Exercise Science and Medicine, University of Glasgow, Glasgow, United Kingdom; <sup>8</sup>Cancer Research UK Cambridge Research Institute, Li Ka Shing Centre, Cambridge, United Kingdom; <sup>9</sup>Department of Computer Science, University of Warwick, Coventry, United Kingdom; and <sup>10</sup>Department of Musculoskeletal Biology and Magnetic Resonance & Image Analysis Research Centre, University of Liverpool, Liverpool, United Kingdom

Submitted 26 April 2013; accepted in final form 22 June 2013

**Cannon DT, Howe FA, Whipp BJ, Ward SA, McIntyre DJ, Ladroue C, Griffiths JR, Kemp GJ, Rossiter HB.** Muscle metabolism and activation heterogeneity by combined  $^{31}\text{P}$  chemical shift and  $T_2$  imaging, and pulmonary  $\text{O}_2$  uptake during incremental knee-extensor exercise. *J Appl Physiol* 115: 839–849, 2013. First published June 27, 2013; doi:10.1152/jappphysiol.00510.2013.—The integration of skeletal muscle substrate depletion, metabolite accumulation, and fatigue during large muscle-mass exercise is not well understood. Measurement of intramuscular energy store degradation and metabolite accumulation is confounded by muscle heterogeneity. Therefore, to characterize regional metabolic distribution in the locomotor muscles, we combined  $^{31}\text{P}$  magnetic resonance spectroscopy, chemical shift imaging, and  $T_2$ -weighted imaging with pulmonary oxygen uptake during bilateral knee-extension exercise to intolerance. Six men completed incremental tests for the following: 1) unlocalized  $^{31}\text{P}$  magnetic resonance spectroscopy; and 2) spatial determination of  $^{31}\text{P}$  metabolism and activation. The relationship of pulmonary oxygen uptake to whole quadriceps phosphocreatine concentration ([PCr]) was inversely linear, and three of four knee-extensor muscles showed activation as assessed by change in  $T_2$ . The largest changes in [PCr], [inorganic phosphate] ([Pi]) and pH occurred in rectus femoris, but no voxel (72  $\text{cm}^3$ ) showed complete PCr depletion at exercise cessation. The most metabolically active voxel reached  $11 \pm 9$  mM [PCr] (resting,  $29 \pm 1$  mM),  $23 \pm 11$  mM [Pi] (resting,  $7 \pm 1$  mM), and a pH of  $6.64 \pm 0.29$  (resting,  $7.08 \pm 0.03$ ). However, the distribution of  $^{31}\text{P}$  metabolites and pH varied widely between voxels, and the intervoxel coefficient of variation increased between rest ( $\sim 10\%$ ) and exercise intolerance ( $\sim 30\text{--}60\%$ ). Therefore, the limit of tolerance was attained with wide heterogeneity in substrate depletion and fatigue-related metabolite accumulation, with extreme metabolic perturbation isolated to only a small volume of active muscle ( $<5\%$ ). Regional intramuscular disturbances are thus likely an important requisite for exercise intolerance. How these signals

integrate to limit muscle power production, while regional “re-cruitable muscle” energy stores are presumably still available, remains uncertain.

skeletal muscle; exercise; quadriceps; magnetic resonance spectroscopy; oxygen uptake

TOLERANCE TO WHOLE BODY EXERCISE is a major determinant of quality of life and mortality (42). However, the mechanisms limiting exercise tolerance are poorly understood. Skeletal muscle substrate depletion and other intramuscular metabolic changes contribute directly to limiting muscle power production (15). In addition, increased muscle energetic requirements may also contribute indirectly to exercise intolerance through a sense of effort, or by causing systemic metabolic disturbances that alter, for example, blood flow ( $\dot{Q}$ ) distribution, ventilation, the work of breathing, dyspnea, and/or pain (23). Reserves of whole muscle intramuscular energy stores [e.g., phosphocreatine (PCr) and adenosine triphosphate (ATP)] often remain at volitional exhaustion during large muscle mass exercise, such as bilateral knee/hip extension or cycle ergometry (22, 49). However, the magnitude of local variation in metabolic strain, and therefore whether the relevant muscles remain energetically competent to produce the required power during large muscle-mass exercise, remains obscure.

Human single muscle fibers sampled through biopsy manifest a wide distribution of metabolite concentrations during high-intensity exercise, with PCr concentration ([PCr]) in some fibers approaching the limit of detection even before the limit of tolerance (32). However, the extent to which these limiting conditions in a small biopsy reflect heterogeneous metabolic responses across the involved muscle group during exercise is not clear. While single-site metabolite estimates from biopsy (55) provide highly specific and localized information from the presumed most energetically challenged region of the muscle, measures such as muscle-venous blood sampling (which rep-

† Deceased.

Address for reprint requests and other correspondence: H. B. Rossiter, Division of Respiratory & Critical Care Physiology & Medicine, Los Angeles Biomedical Research Institute at Harbor-UCLA Medical Center, 1124 W Carson St, CDCRC Bldg., Torrance, CA 90502 (e-mail: hrossiter@ucla.edu).

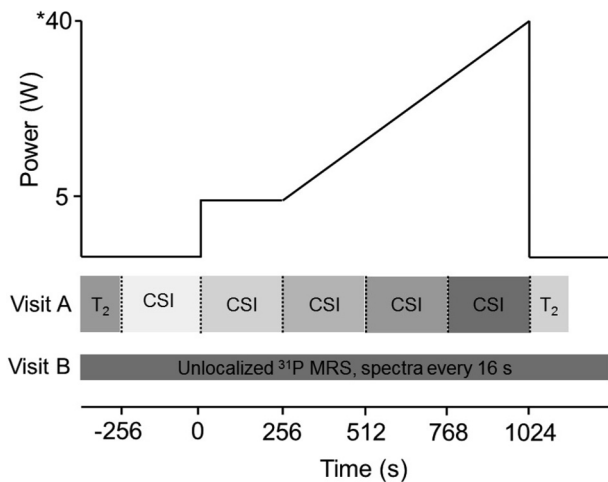


Fig. 1. Composite schematic of the measurement protocols during two ramp incremental exercise tests. The protocol consisted of a resting stage, a 5-W baseline exercise stage, and a ramp incremental exercise phase tailored to bring about intolerance after 3 complete chemical shift imaging (CSI) stages. For CSI, the data-acquisition stages each lasted 256 s. On the y-axis, \* denotes an example peak power, but this varied for each participant. T<sub>2</sub>, transverse relaxation time; MRS, magnetic resonance spectroscopy.

resents a flow-weighted mean) or unlocalized<sup>1</sup> <sup>31</sup>P magnetic resonance spectroscopy [(MRS) (52)] interrogate relatively large regions of heterogeneous muscle. During single-leg exercise, unlocalized <sup>31</sup>P-MRS data suggest that exercise limitation coincides with a challenge to the muscle [PCr] as it approaches the limit of detection (58). It remains unclear, however, how much whole muscle, or even regional muscle, substrate depletion may occur during exercise with a larger involved muscle mass, where the systemic challenge to homeostasis and the influence of muscle afferent feedback is heightened. The combination of the heterogeneity in muscle metabolism and the technical limitations of available sampling methods greatly confound the in vivo characterization of skeletal muscle fatigue-related changes in relation to exercise limitation in large muscle-mass exercise. A “middle ground” of spatial resolution is offered by <sup>31</sup>P chemical shift imaging (CSI), which may shed light on this complexity.

Detecting localized metabolic disturbances during exercise is possible with <sup>31</sup>P-CSI (7). CSI can provide a metabolite map, allowing characterization of metabolism between muscles and within single-muscle regions. The method also can balance a need for spatial resolution against the short acquisition times necessary for the temporal resolution required in non-steady-state exercise. CSI has been used to study leg muscles at rest and in recovery from exercise (16, 27, 41), in forearm (21, 44) and dorsi-/plantar flexor (19, 48) muscles during steady-state exercise, and in the quadriceps muscles during constant-power single-leg exercise and recovery (45), although not during a dynamic bilateral leg activity. In addition, muscle metabolic heterogeneity at the limit of tolerance will reflect the diversity of muscle recruitment, as well as the biochemistry of supporting energy conversion. The tissue water spin-spin transverse relaxation time (T<sub>2</sub>) from <sup>1</sup>H magnetic resonance imaging

(MRI) provides the opportunity to estimate muscle activation patterns (1) in relation to measures of local (<sup>31</sup>P-CSI) and whole body [pulmonary oxygen uptake ( $\dot{V}O_2$ )] metabolism during bilateral leg exercise in the bore of a superconducting magnet (62).

Our aim was, therefore, to characterize the dynamic inter-relationships between whole body  $\dot{V}O_2$ , whole and regional quadriceps <sup>31</sup>P metabolism and intracellular pH (pH<sub>i</sub>), together with muscle activation by <sup>1</sup>H-MRI, across the full range of exercise intensity. To achieve this, we used <sup>31</sup>P-CSI of one thigh and T<sub>2</sub>-weighted <sup>1</sup>H MRI of the other thigh during bilateral ramp-incremental knee extension to the limit of tolerance. We hypothesized that localized measurements would reveal potential regional metabolic limitation, which is obscured by traditional global measures of metabolism ( $\dot{V}O_2$ ) and whole quadriceps <sup>31</sup>P-MRS.

## MATERIALS AND METHODS

**Ethical approval.** The ethics committee at St. George’s Hospital Trust, London, approved this study, and all procedures complied with the latest revision of the Declaration of Helsinki. Written, informed consent was obtained from all volunteers before their participation in the study.

**Participants and exercise protocols.** Six healthy, active men were recruited for this study (mean ± SD: 24 ± 3 yr; 184 ± 3 cm; 88 ± 7.6 kg). Participants were screened for known disease and completed an exercise history and a physical activity readiness questionnaire.

All exercise tests were completed on a magnetic resonance (MR)-compatible, computer-controlled electromagnetically braked knee-extension ergometer (MRI Ergometer Up/Down, Lode BV, Groningen, the Netherlands). The participants lay prone with their feet strapped into molded plastic stirrups attached to aluminum arms linking the ergometer cranks. Their hips were secured to the scanner bed with padded nylon and Velcro straps to minimize hip flexion/extension. This setup, similar to an exercise model previously described (62), allowed for ~35° (limited by the scanner bore) of bilateral, alternate knee-flexion/extension to drive an electromagnetically braked flywheel. No resistance was present during knee flexion, other than the work required to lift the mass of the lower leg.

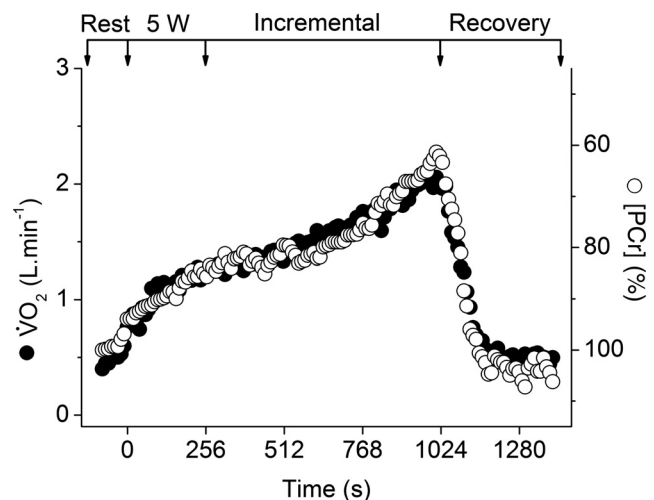


Fig. 2. Profile of O<sub>2</sub> uptake ( $\dot{V}O_2$ ; ●) and whole-quadriceps unlocalized phosphocreatine concentration ([PCr]; ○) during the ramp incremental exercise phase in a representative participant. Arrows represent the beginning/end of 5-W and ramp incremental phases. [PCr] is given as percentage of resting, with the y-axis inverted to show more clearly the relationship to  $\dot{V}O_2$ .

<sup>1</sup> While <sup>31</sup>P-MRS is, by definition, surface-coil localized, we will refer to it as “unlocalized” throughout the paper.

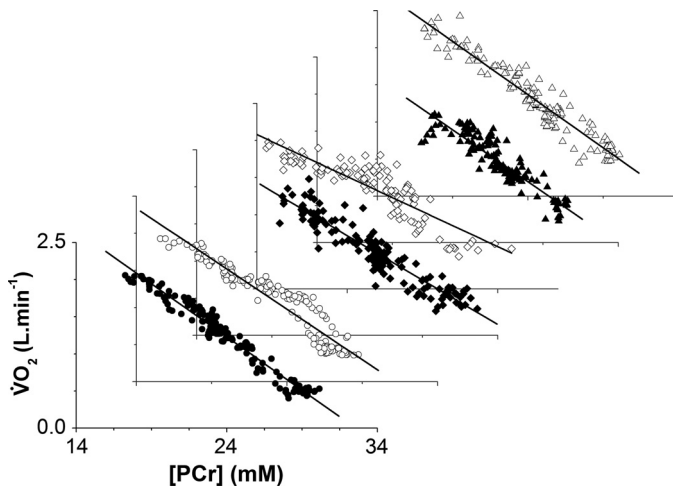


Fig. 3. Profiles of the  $\dot{V}O_2$ -[PCr] relationship during the ramp incremental exercise and recovery in 6 participants. Resting and recovery data are included. [PCr] is given as an absolute concentration. A linear regression line is shown for each individual data set. For clarity, the symbols represent different participants.

Once familiarized, the physiological responses to this exercise mode are reproducible between visits in the same subjects (62). Therefore, each participant underwent a comprehensive series of familiarization visits to account for learning effects and also to ensure consistent muscle activation patterns among multiple MR measurements. Participants completed up to six ramp incremental tests until exercise responses could be reproduced on three successive occasions.

For the MR measurements, participants completed two ramp incremental exercise tests in a random order on separate days for 1) CSI and  $T_2$  imaging; and 2) unlocalized  $^{31}\text{P}$ -MRS. Participants lay at rest, followed by a baseline exercise phase at 5 W. The power was then increased continuously at a rate (2–3 W/min), tailored to each participant, to produce task failure in  $\sim 12$  min. This allowed for three complete CSI acquisitions during ramp incremental exercise (Fig. 1). The frequency of bilateral knee extension was 60 cycles/min, synchronized with  $^{31}\text{P}$ -MRS acquisition. Audible clicks within the scanner were achieved by including a pulsed spoiler gradient at the end of each MRS acquisition. Exercise was terminated when the participant could no longer maintain the required cadence, despite strong verbal encouragement. Participants lay still in the MR scanner for 5 min resting recovery, for  $^{31}\text{P}$ -MRS (following the unlocalized protocol) and thigh  $T_2$  image acquisition (following the CSI protocol). Pulmonary  $\dot{V}O_2$  was simultaneously measured breath by breath (62).

$^{31}\text{P}$ -MRS. Muscle phosphorus-containing metabolites were measured with a 1.5T superconducting magnet (Signa Advantage, GE Healthcare, Milwaukee, WI). A one-pulse  $^{31}\text{P}$ -MRS acquisition was employed with an 8 in./5 in. transmit/receive surface coil placed under

the knee extensors [rectus femoris (RF), vastus medialis (VM), vastus intermedius (VI), and vastus lateralis (VL)] of the dominant leg (the right leg in all subjects), halfway between hip and knee. A series of axial gradient-recalled echo images of the thigh confirmed coil placement relative to the knee-extensor muscles. Before the  $^{31}\text{P}$  acquisitions, the magnetic field homogeneity was optimized using the localized water signal from a large volume of quadriceps muscles enclosing the sensitive region of the  $^{31}\text{P}$  coil.

Unlocalized  $^{31}\text{P}$  free induction decays were collected from the quadriceps with a repetition time (TR) of 2 s throughout the rest-exercise-recovery protocol.  $^{31}\text{P}$  data were averaged over eight free induction decay acquisitions, yielding a spectrum every 16 s to estimate the signal intensities of Pi, PCr,  $\gamma$ -ATP,  $\alpha$ -ATP, and  $\beta$ -ATP.

During the ramp incremental protocol, spatially resolved acquisition relied on  $^{31}\text{P}$ -CSI with 8-cm slice thickness,  $16 \times 16$  phase encoding steps, and a  $48\text{-cm}^2$  field of view. The volume of each voxel was  $3 \times 3 \times 8$  cm, or  $72\text{ cm}^3$ , and voxel selection for specific muscles was done with reference to the multislice MRI. A TR of 1 s was used, and a two-dimensional  $^{31}\text{P}$  metabolite map was generated every 256 s. This acquisition time was determined from pilot measurements to ensure good spectral data from the quadriceps and represents an optimal compromise between signal-to-noise, temporal resolution, and spatial resolution.

*Data analyses for  $^{31}\text{P}$  measures.* Signal intensities, frequencies, and line widths of Pi, PCr, and ATP were quantified using Java-based version of the magnetic resonance user interface (43). Uncalibrated concentrations for PCr and Pi were determined from assuming  $\beta$ -ATP concentration of 8.2 mM (28, 54).  $\text{pH}_i$  was estimated from the chemical shift of Pi (40):

$$\text{pH} = 6.75 + \log(\delta - 3.27/5.69 - \delta) \quad (1)$$

where  $\delta$  is the chemical shift of the Pi peak relative to PCr. In the case of Pi peak splitting (51, 57), a Pi signal intensity-weighted mean of the two pH values was used for analyses (53).

$^{31}\text{P}$ -CSI postprocessing was done using SAGEIDL software (GE, Milwaukee, WI, version dev2000.3) to allow for voxel shifting to the proper region of tissue to characterize the knee-extensor muscles. Signal intensities, frequencies, and line widths were transformed into a time series for each region of interest on the  $^{31}\text{P}$  metabolite map.

$^1\text{H}$ -MRI. At rest and immediately following the limit of tolerance,  $T_2$ -weighted  $^1\text{H}$  images were obtained with the whole body imaging coil and used to estimate muscle activation. Changes in the spin-spin relaxation time,  $T_2$  ( $\Delta T_2$ ) from rest to peak exercise were used to estimate relative muscle activation during ramp incremental exercise. The  $^{31}\text{P}$  surface coil under the right quadriceps caused artifact in the  $T_2$  image, and, therefore,  $\Delta T_2$  was determined in the muscles of the left leg. Quantitative apparent- $T_2$  maps were constructed pixel by pixel from dual-fast-spin echo  $^1\text{H}$  images (TR of 4,000 ms; echo times of 30 and 63 ms), assuming exponential decay, and quantified from the average of the density map within each quadriceps muscle. Scan time for  $T_2$  imaging was 176 s.

Table 1.  $T_2$  at rest and immediately after the limit of tolerance in the muscles of the quadriceps

Participant No.	RF		VM		VI		VL	
	Preexercise	Postexercise	Preexercise	Postexercise	Preexercise	Postexercise	Preexercise	Postexercise
1	45	49	52	51	63	64	63	52
2	48	63	51	55	59	62	52	75
3	46	62	49	52	63	66	54	56
4	46	70	51	57	61	60	56	63
5	49	55	46	49	47	57	35	51
6	47	50	48	45	49	49	49	51
Mean (SD)	47 (2)	58 (8)*	49 (2)	52 (4)	57 (7)	60 (6)	51 (9)	58 (10)

Values are in ms.  $T_2$ , spin-spin relaxation time; RF, rectus femoris; VM, vastus medialis; VI, vastus intermedius; VL, vastus lateralis. Different from the preexercise value (\* $P = 0.02$ ).



Table 2.  $\Delta T_2$  in the muscles of the quadriceps

Participant No.	Largest $\Delta T_2$		2nd Largest $\Delta T_2$		2nd Smallest $\Delta T_2$		Smallest $\Delta T_2$	
	$\Delta T_2$	Muscle	$\Delta T_2$	Muscle	$\Delta T_2$	Muscle	$\Delta T_2$	Muscle
1	4	RF	1	VI	-1	VM	-11	VL
2	23	VL	15	RF	4	VM	3	VI
3	16	RF	3	VM	3	VI	2	VL
4	24	RF	7	VL	6	VM	-1	VI
5	16	VL	10	VI	6	RF	3	VM
6	3	RF	2	VL	0	VI	-3	VM
Mean (SD)		14 (9) <sup>†</sup>		6 (5) <sup>*†</sup>		3 (3) <sup>‡</sup>		-1 (5) <sup>§</sup>

Difference in  $T_2$  relaxation times between rest and immediately after the limit of tolerance ( $\Delta T_2$ ). Values are presented in ms and ordered from largest to smallest  $\Delta T_2$ . Different from the next largest rank-ordering of  $\Delta T_2$  (\* $P = 0.02$ , § $P = 0.03$ ). Different from zero (<sup>†</sup> $P = 0.05$ , <sup>‡</sup> $P = 0.06$ ).

**Pulmonary gas exchange.** Participants breathed through a low-resistance (<0.1 kPa·l<sup>-1</sup>·s<sup>-1</sup> at 15 l/s), low-dead-space (90 ml) mouthpiece for the measurement of respired gases, as previously described (62). Flow rates and volumes were measured with a custom-designed nonmagnetic turbine flow sensor (VMM, Interface Associates, Laguna Niguel, CA), while a quadrupole mass spectrometer measured gas concentrations from respired gas sampled from the mouthpiece (QP9000; CaSE, Gillingham, Kent, UK). During the <sup>31</sup>P-MRS experiment, the mass spectrometer and computer were housed in the scanner control room, outside the Faraday cage. The volume transducer signal was filtered to prevent conduction of radio frequency noise into the scanner room. Due to the length of the respired gas capillary tubing (13.7 m), the measured time delay between the near-instantaneous turbine flow signal and the gas concentration signals was used to align the signals for breath-by-breath analysis (6). This increase in transit delay and sample line length did not influence the 5–95% rise time of the quadrupole mass spectrometer or the signal fidelity of respired gases (62).

The flow sensor and gas analyzers were calibrated before each experiment. The turbine volume transducer was calibrated in the bore of the scanner with a 3-liter syringe (Hans Rudolph, Shawnee, KS). The calibration was completed with flow rates ranging from 0.2 to 6 l/s, mimicking flow rates expected for humans at rest and during exercise. After the completion of the flow sensor calibration, the flow volumes were verified over 25 syringe strokes of varying flow rates and accepted when the means were within  $\pm 0.01$  l, with a SD and coefficient of variation (CV) of 0.02 l and 1%, respectively. Additionally, the mass spectrometer was calibrated with two high-precision-certified gases (BOC Group, Guildford, UK) with concentrations of O<sub>2</sub>, CO<sub>2</sub>, and N<sub>2</sub> spanning the physiological range (O<sub>2</sub>, 21 and

10%; CO<sub>2</sub>, 0 and 8%; N<sub>2</sub>, 79 and 82%), and verified using room air. Following each experiment, the mass spectrometer calibrations were checked by resampling the calibration gases.

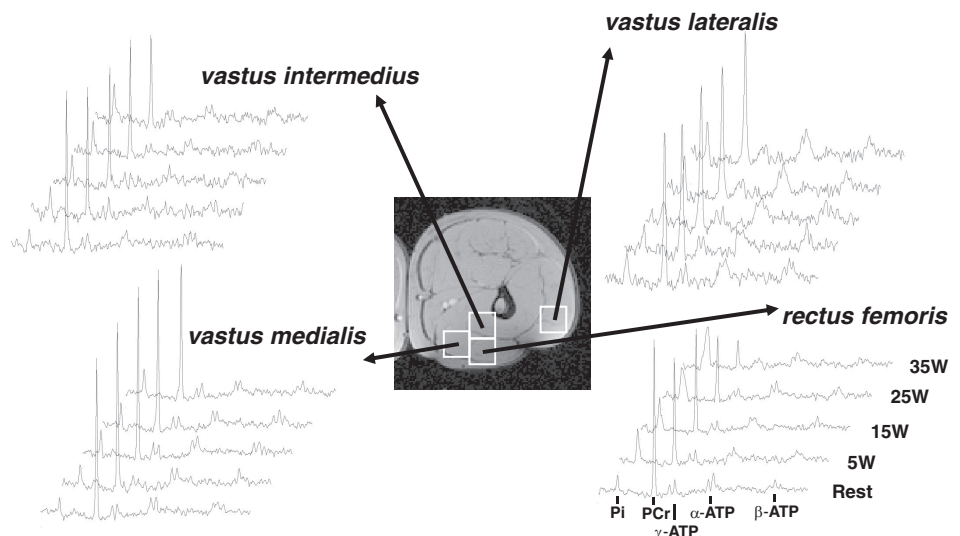
**Data analyses for pulmonary gas exchange.** To improve signal to noise,  $\dot{V}O_2$  breath-by-breath data were filtered by removing values residing more than 4 SD from the local mean. Data were time aligned, interpolated, averaged into 10-s bins, and ensemble averaged across like transitions. Peak values were calculated from 20-s means immediately before the limit of tolerance.

**Statistical analyses.** Changes in  $\dot{V}O_2$ , muscle activity, and metabolites with exercise were assessed with repeated-measures ANOVA or paired *t*-test, where appropriate. Heterogeneity was characterized using a normalized dispersion, or CV (expressed as %). Statistics were completed using the Statistical Package for the Social Sciences (SPSS v17.0, SPSS, Chicago, IL).

## RESULTS

During ramp incremental exercise, participants achieved a peak power of  $42 \pm 10$  W, which was reproducible within  $2 \pm 2$  W. Following an initial kinetic phase,  $\dot{V}O_2$  rose progressively to achieve a peak  $\dot{V}O_2$  of  $1.98 \pm 0.30$  l/min, which equated to ~55% of cycling maximum  $\dot{V}O_2$  in these participants. Consequently, the dynamic  $\dot{V}O_2$ -[PCr] relationship from the unlocalized <sup>31</sup>P-MRS measurements was approximately linear in all participants (Figs. 2 and 3). The mean slope and intercept of this relationship were  $-0.13 \pm 0.02$  l·min<sup>-1</sup>·mM<sup>-1</sup> and  $4.34 \pm 0.53$  l/min, respectively. The CV for the slope and intercept of the  $\dot{V}O_2$ -[PCr] were ~15% for each of the partic-

Fig. 4. <sup>31</sup>P-MRS stack plots acquired by CSI in a representative participant during each stage of the exercise protocol from 4 voxels placed in each of the 4 knee-extensor muscles labeled. <sup>31</sup>P-MR spectra, from bottom to top, represent rest, 5-W baseline exercise, and three acquisitions during ramp incremental exercise. Visible in the spectra are the peaks (chemical shift from left to right) for Pi, PCr,  $\gamma$ -ATP,  $\alpha$ -ATP, and  $\beta$ -ATP. The two-dimensional <sup>1</sup>H magnetic resonance image was used to identify voxel positioning.



ipants, with the regression function for five of the participants showing a slope and intercept CV of  $\sim 7\%$ .

Resting [PCr], [Pi], and  $\text{pH}_i$  from unlocalized MRS were  $29 \pm 1$  mM,  $7 \pm 1$  mM, and  $7.08 \pm 0.03$ , respectively. At peak exercise, [PCr], [Pi], and  $\text{pH}_i$  were  $20 \pm 4$  mM,  $19 \pm 5$  mM, and  $6.91 \pm 0.08$ . Therefore, from rest to peak exercise, [PCr] decreased by  $9 \pm 4$  mM ( $P = 0.002$ ), [Pi] increased by  $12 \pm 4$  mM ( $P = 0.001$ ), and  $\text{pH}_i$  decreased ( $P = 0.001$ ) by  $0.18 \pm 0.07$ .

$T_2$  imaging revealed activation variability in the four quadriceps muscles contributing to the exercise. In the RF muscle,  $T_2$  increased from rest to exercise ( $47 \pm 1.6$  vs.  $58 \pm 8.2$  ms;  $P = 0.02$ ), while no change was detected in the VM muscle ( $P = 0.15$ ), VI ( $P = 0.22$ ), or VL ( $P = 0.22$ ) (Table 1). However, this approach obscured individual differences in  $T_2$  changes among muscles, as there was a considerable variability in activation pattern of the knee extensors among participants (24). Therefore, the postexercise muscle activation was ranked from largest to smallest  $T_2$  change for each participant. A significant main effect was present in ranked muscle activation by  $\Delta T_2$  ( $F = 5.9$ ;  $P = 0.007$ ;  $\eta^2 = 0.54$ ), with two of four rank orderings different from one another (Table 2), indicating large variability in activation among muscles. Additionally, three of four muscles showed a  $\Delta T_2$  that was different from zero, indicating that at least three of the four knee-extensor muscles were active (to varying degrees) in each participant (Table 2). At the limit of tolerance,  $T_2$  heterogeneity in each participant was  $-21\%$  to  $+32\%$  of the knee-extensor mean  $T_2$ .

[PCr], [Pi], and  $\text{pH}_i$  changes from rest to end-exercise varied considerably across the knee-extensor muscles (Figs. 4, 5, and 6). The largest changes in each variable occurred in the RF muscle, with a significant interaction (power  $\times$  muscle) present ( $F = 10.0$ ;  $P = 0.02$ ;  $\eta^2 = 0.67$ ). No single voxel showed "complete" depletion of PCr; the lowest concentration (in RF) reaching  $\sim 8$  mM in three participants (Fig. 7). The CV for  $^{31}\text{P}$  metabolites at each power across the knee-extensor muscles increased from rest to peak exercise ([PCr],  $11 \pm 5$  vs.  $30 \pm 12\%$ ,  $P = 0.01$ ; [Pi],  $35 \pm 9$  vs.  $63 \pm 22\%$ ,  $P = 0.03$ ). The relatively small CV for  $\text{pH}_i$  ( $\sim 1\text{--}4\%$ ) reflects its logarithmic scale; thus, for  $[\text{H}^+]$ , CV increased from rest to peak exercise ( $6 \pm 3$  vs.  $34 \pm 26\%$ ;  $P = 0.04$ ). As the CSI metabolite maps are a mean of the entire  $\sim 4$ -min acquisition, the trajectories of metabolite changes were extrapolated to exercise cessation using linear regression between the final two CSI acquisitions in the ramp incremental protocol (Figs. 5 and 6). At the point of intolerance [PCr], [Pi], and  $\text{pH}_i$  in the RF were extrapolated to  $11 \pm 9$  mM (or  $36 \pm 27\%$  resting),  $23 \pm 11$  mM, and  $6.64 \pm 0.29$ , respectively. Extrapolated [PCr] in two participants was reduced to 3.5 mM, or  $\sim 10\%$  of resting [PCr] (e.g., Fig. 5).

At peak exercise, Pi peak splitting was evident in the RF voxel of all six participants. Additionally, all participants showed at least three of four knee extensors with Pi peak splitting during exercise. When  $\text{pH}_i$  was calculated from the chemical shift of Pi, the difference at peak exercise for the split Pi voxels in the RF muscle was  $6.70 \pm 0.23$  vs.  $6.92 \pm 0.18$  ( $P = 0.0006$ ).

The changes in [PCr], [Pi], and  $\text{pH}_i$  from rest to end exercise were used to rank the four muscles of the quadriceps in order of metabolic disturbance, as described above for  $T_2$ . A significant effect was present for ranked  $\Delta[\text{PCr}]$  ( $F = 13.8$ ;  $P = 0.01$ ;  $\eta^2 = 0.74$ ),  $\Delta[\text{Pi}]$  ( $F = 19.5$ ;  $P = 0.004$ ;  $\eta^2 = 0.80$ ), and

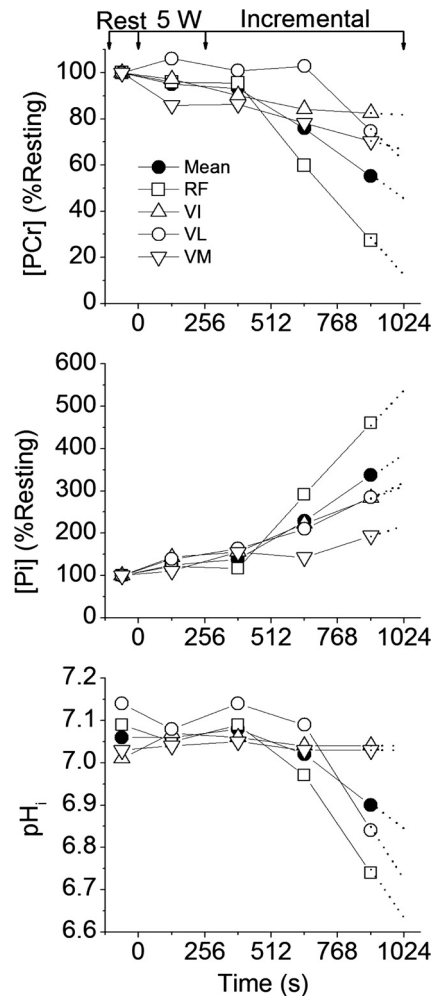


Fig. 5. Profiles for [PCr], [Pi], and intracellular pH ( $\text{pH}_i$ ) measured by CSI in a representative participant in the 4 knee-extensor muscles: rectus femoris (RF; □); vastus intermedius (VI; △); vastus lateralis (VL; ○); vastus medialis (VM; ▽). Also shown is the mean of the 4 muscles (●). Arrows represent the beginning/end of 5-W and ramp incremental phases. [PCr] and [Pi] are expressed as a percentage of their resting values. Dotted lines show linear regression extrapolation to the limit of tolerance.

$\Delta\text{pH}_i$  ( $F = 9.9$ ;  $P = 0.02$ ;  $\eta^2 = 0.66$ ) (Tables 3, 4, and 5). This analysis indicated that the metabolic disturbance in the four muscles (reduction in [PCr], and increase in [Pi]) was significantly different from one another (Tables 3 and 4). This was also the case for  $\Delta\text{pH}_i$ , except that the two muscles showing the greatest change (mostly RF and VL) were not different from each other (Table 5).

## DISCUSSION

*Activation of the knee extensors and regional metabolism.* The lagged profiles of whole body  $\dot{V}\text{O}_2$  and unlocalized [PCr] were consistent with an approximately exponential response to the linear power forcing (Fig. 2). The resulting slopes of the linear phase of the dynamic  $\dot{V}\text{O}_2$ -[PCr] relationship were similar among participants, reflecting that the whole-muscle oxidative capacity, total creatine concentration, and ATP rephosphorylated per  $\frac{1}{2}$   $\text{O}_2$  reduced (P/O) varied only slightly among these young healthy individuals (37) (Fig. 3). However, consistent with our hypothesis, this linearity obscured a wide

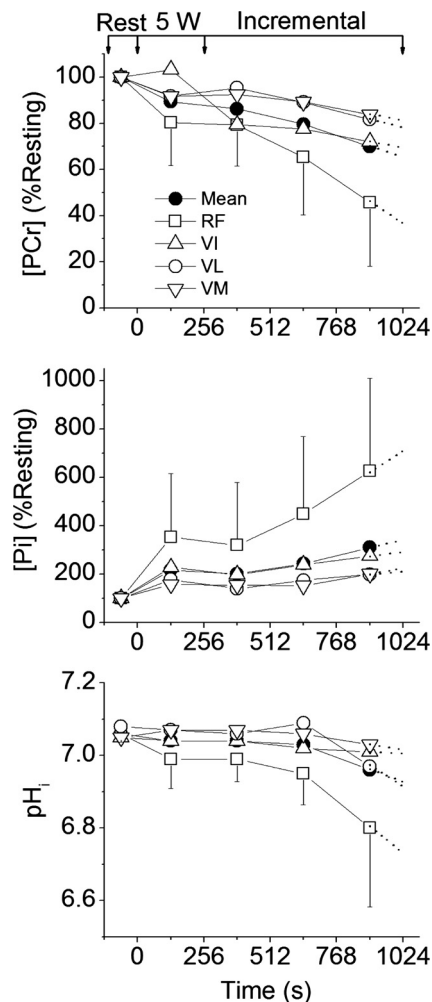


Fig. 6. Group means for [PCr], [Pi], and  $\text{pH}_i$  measured by CSI in the 4 knee-extensor muscles: RF, VI, VL, VM. Also shown is the mean of the 4 muscles. Symbols are as defined in Fig. 5 legend. Arrows represent the beginning/end of 5-W and ramp incremental phases. Error bars for the VI, VL, and VM are omitted for clarity, but show similar distribution to the RF. Dotted lines show linear regression extrapolation to the limit of tolerance.

distribution of  $^{31}\text{P}$  metabolite changes across the knee-extensor muscles during ramp incremental exercise, which was revealed by localized  $^{31}\text{P}$ -CSI (Figs. 6 and 7). The heterogeneity of [PCr] and [Pi] between individual muscles approximately tripled from rest to the limit of tolerance, and the heterogeneity of  $[\text{H}^+]$  increased approximately fivefold.

This “metabolic strain” is related to muscle activation and the metabolic properties of the muscle region. Muscle activation was assessed in the present study by the change in  $T_2$  (38).  $\Delta T_2$  reflects mainly the accumulation of osmotically active ions and water associated with muscle activation (1). During our knee-extensor exercise protocol, over the range of extension from  $\sim 145$  to  $180^\circ$ , the greatest disturbance to [PCr], [Pi], and  $\text{pH}_i$  (Figs. 5 and 6) and  $\Delta T_2$  (Table 2) was most commonly seen in the RF muscle. However, muscle activation patterns were highly variable among individuals for this exercise mode, prompting comparisons using the rank order of muscle activity. Using this approach, at the limit of tolerance, three of four knee-extensor muscles showed at least some activation ( $\Delta T_2$  different from zero;

Table 2), consistent with being biomechanically “available” to contribute to power production during prone knee extension. Importantly, and contrary to our hypothesis, no single muscle region showed complete depletion of [PCr], even when responses were extrapolated to end-exercise from the time of the CSI acquisitions. Thus, our principal finding is that the limit of tolerance was reached with an apparent energy reserve of  $\sim 10\%$  of [PCr] in the most metabolically active muscle region, with heterogeneous metabolic responses across the active muscle group.

*Considerations for spatial resolution.* The interacting constraints on spatial and temporal resolution for CSI are a potential limitation of our study. The voxel sizes ( $72\text{ cm}^3$ ) equate to  $\sim 80\text{ g}$  of tissue (assuming a muscle tissue density of  $\sim 1.1\text{ g/cm}^3$ ), rendering CSI a “blunt” tool compared with biopsy. The single-voxel mass ( $\sim 5\%$  of the active muscle) greatly exceeds that of muscle biopsy ( $\sim 0.005\%$  of active muscle) where single fibers have been reported with near-complete PCr depletion (31). To this point, numerous voxels in the present study exhibited Pi peak splitting, consistent with previous measurements (57), suggesting that intravoxel compartmentalization of metabolites was present in our

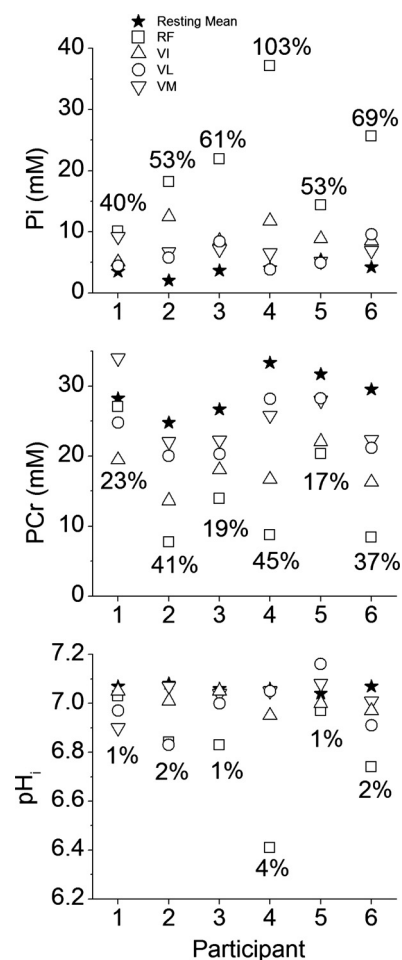


Fig. 7. Individual participant data for [PCr], [Pi], and  $\text{pH}_i$  measured by CSI at peak exercise in the 4 knee-extensor muscles: RF, VI, VL, VM. Symbols are as defined in Fig. 5 legend. The resting value (★) is the mean of all 4 knee extensors. Coefficients of variation are presented as a percentage on each panel and represent the value at peak exercise.

Table 3.  $\Delta[\text{PCr}]$  in the muscles of the quadriceps

Participant No.	Largest $\Delta[\text{PCr}]$		2nd Largest $\Delta[\text{PCr}]$		2nd Smallest $\Delta[\text{PCr}]$		Smallest $\Delta[\text{PCr}]$	
	$\Delta[\text{PCr}]$	Muscle	$\Delta[\text{PCr}]$	Muscle	$\Delta[\text{PCr}]$	Muscle	$\Delta[\text{PCr}]$	Muscle
1	9.6	VI	6.5	RF	3.5	VM	2.2	VL
2	15.1	RF	7.9	VI	6.7	VL	5.4	VM
3	16.5	RF	8.9	VI	5.3	VM	3.5	VL
4	27.2	RF	10.3	VI	2.9	VM	-4.0	VL
5	10.6	RF	9.9	VI	5.7	VL	3.2	VM
6	20.3	RF	13.7	VI	10.3	VM	5.7	VL
Mean (SD)	16.5 (6.5)		9.5 (2.5)*		5.7 (2.7)†		2.7 (3.6)‡	

Difference in phosphocreatine concentration between rest and end-exercise ( $\Delta[\text{PCr}]$ ) values are presented in mM and ordered from largest to smallest  $\Delta[\text{PCr}]$ . Different from the next largest rank-ordering of  $\Delta[\text{PCr}]$  (\* $P = 0.03$ , † $P = 0.01$ , ‡ $P = 0.02$ ).

data. Nevertheless, our data show that only very small, localized muscle regions are likely to demonstrate metabolically limiting conditions at the limit of tolerance during bilateral leg exercise. It also provides an important additional frame of reference for the distribution of the metabolic disturbance within the muscle mass available for exercise. This is because the data suggest that the true proportion of muscle mass reaching metabolically limiting conditions resides in between the resolutions of the CSI used here and the muscle biopsy technique.

From available biopsy data, ~10% of muscle fibers in the sample exhibit [PCr] approaching zero (operationally, <5 mmol/kg dry mass) when sampled after submaximal heavy exercise (31); these fibers were part of a distribution with a mean [PCr] of ~30 mmol/kg dry mass with a CV of ~15% (31). Our data show a mean extrapolated [PCr] in the RF muscle at the limit of tolerance of ~10 mM (wet mass), with a CV of ~30%. Therefore, given the values from biopsy studies, it seems reasonable to suggest that [PCr] will approach zero in at least 10% of the muscle fibers within a highly metabolically active voxel. However, not all voxels characterizing the active muscle showed this magnitude of metabolic challenge. Across the entire mass engaged in exercise, the true regions with intracellular conditions limiting force production may be far smaller than local biopsy results suggest, and probably of the order of <5%, dispersed widely through the muscle i.e., PCr is depleted in ~10% of the fibers within only one of the four active quadriceps muscles measured by CSI. In other words, intramuscular metabolic conditions that would severely impair muscle power production during voluntary large muscle-mass exercise are observed only in a very limited fraction of the recruited muscle. Whether these conditions, in very small

muscle volumes, contribute to bringing about task failure remains unclear.

*Heterogeneity in skeletal muscle perfusion and metabolism during exercise.* Within a limb muscle region during exercise, or even within a single muscle (13),  $\dot{Q}$  is unevenly distributed, which has the potential to disrupt oxygen transport and mitochondrial oxygen utilization (47). During isometric knee-extension in humans, the quadriceps muscle exhibits a wide heterogeneity of  $\dot{Q}$  (25). Our data also show wide variation in metabolic changes, with the RF muscle exhibiting the largest disturbance. Whether these two dispersions are well matched, or even related, remains uncertain.

The matching of  $\dot{Q}$  to  $\dot{V}\text{O}_2$  is an important determinant of exercise tolerance (46, 61), so there is considerable interest in measuring both variables with high temporal and spatial resolution. Due to the technical constraints in achieving the required resolutions, this has proven to be a difficult task, even while at rest (39). Unlike in the myocardium (35) or brain (34), there appears to be little or no relationship between local  $\dot{Q}$  and metabolism (i.e., as judged by glucose uptake or PCr breakdown) in exercising skeletal muscle (20, 26, 36, 48). This is in contrast to measures made during rest and exercise-recovery in which  $\dot{Q}$ - $\dot{V}\text{O}_2$  matching was relatively homogenous (39), or in the case of estimating metabolic activity from free fatty acid uptake, which was correlated with  $\dot{Q}$  (36). Measuring spatially resolved  $\dot{Q}$  with arterial spin labeling (ASL) in concert with PCr measurement in humans (48) showed a poor relationship of perfusion to metabolism, although differences in oxidative capacity between muscle regions complicate interpretation of these comparisons. Also, volume changes, movement artifact, and fluid redistribution each present a substantial

Table 4.  $\Delta[\text{Pi}]$  in the muscles of the quadriceps

Participant No.	Largest $\Delta[\text{Pi}]$		2nd Largest $\Delta[\text{Pi}]$		2nd Smallest $\Delta[\text{Pi}]$		Smallest $\Delta[\text{Pi}]$	
	$\Delta[\text{Pi}]$	Muscle	$\Delta[\text{Pi}]$	Muscle	$\Delta[\text{Pi}]$	Muscle	$\Delta[\text{Pi}]$	Muscle
1	7.3	RF	6.1	VM	2.1	VI	-0.3	VL
2	16.5	RF	8.8	VI	4.9	VM	4.5	VL
3	19.7	RF	4.6	VL	4.1	VI	3.4	VM
4	30.3	RF	8.5	VI	3.0	VM	0.5	VL
5	10.1	RF	3.6	VI	2.1	VM	-2.5	VL
6	20.1	RF	6.2	VL	5.5	VI	3.3	VM
Mean (SD)	17.3 (8.2)		6.3 (2.1)*		3.6 (1.4)†		1.5 (2.7)‡	

Difference in Pi concentration between rest and end-exercise ( $\Delta[\text{Pi}]$ ) values are presented in mM and ordered from largest to smallest  $\Delta[\text{Pi}]$ . Different from the next largest rank-ordering of  $\Delta[\text{Pi}]$  (\* $P = 0.01$ , † $P = 0.02$ ).



Table 5.  $\Delta p\text{H}_i$  in the muscles of the quadriceps

Participant No.	Largest $\Delta p\text{H}_i$		2nd Largest $\Delta p\text{H}_i$		2nd Smallest $\Delta p\text{H}_i$		Smallest $\Delta p\text{H}_i$	
	$\Delta p\text{H}_i$	Muscle	$\Delta p\text{H}_i$	Muscle	$\Delta p\text{H}_i$	Muscle	$\Delta p\text{H}_i$	Muscle
1	0.14	VM	0.12	VL	0.06	VI	0.02	RF
2	0.22	RF	0.19	VL	0.05	VI	-0.04	VM
3	0.24	RF	0.06	VL	0.01	VM	-0.01	VI
4	0.61	RF	0.06	VL	0.06	VI	0.02	VM
5	0.10	RF	0.08	VI	-0.01	VM	-0.04	VL
6	0.34	RF	0.19	VL	0.07	VM	0.06	VI
Mean (SD)	0.28 (0.18)		0.12 (0.06)		0.04 (0.03)*		0.002 (0.04)†	

Difference in intramuscular pH between rest and end-exercise ( $\Delta p\text{H}_i$ ) values are ordered from largest to smallest  $\Delta p\text{H}_i$ . Different from the next largest rank-ordering of  $\Delta p\text{H}_i$  (\* $P = 0.01$ , † $P = 0.02$ ).

technical challenge for ASL in contracting skeletal muscle, as opposed to its application to measuring brain Q where these complications are mostly absent (56). Recent reports do show sufficient signal-to-noise with ASL in exercise recovery, where movement artifact and muscle volume change are smaller and slower compared with those during rhythmic contraction (64, 65). However, the estimation of local  $\dot{Q}/\dot{V}\text{O}_2$  during exercise through ASL and CSI has yet to be revisited since the initial methodological report (48). From the limited data available, it appears as though local Q is poorly matched to local metabolism during exercise.

Additional evidence for the regional disruption of the balance between muscle  $\text{O}_2$  delivery and consumption is available using multichannel near-infrared spectroscopy. Near-infrared spectroscopy also indicates a poor relationship between local  $\dot{Q}/\dot{V}\text{O}_2$  with wide distributions in deoxygenation among quadriceps muscle regions during constant-power exercise (deoxygenation amplitude CVs ~10–50%) (29). This is similar to the variation in metabolism for the large locomotor knee-extensor muscles during dynamic exercise observed in our study. However, without simultaneous high-resolution measurements of perfusion, the dynamic  $\dot{Q}$ - $\dot{V}\text{O}_2$  relationships in skeletal muscle remain elusive.

**Potential mechanisms for exercise limitation.** The last measurement in the CSI series represents the regional averages over the final ~4 min of the  $^{31}\text{P}$  dynamics during ramp incremental exercise (Fig. 1). Therefore, the final CSI metabolite map best represents metabolite concentrations at ~2 min before the point of intolerance. When the trajectories of metabolite changes are extrapolated to exercise cessation, assuming linear dynamics (60), an energy reserve still remains within even the most metabolically active muscle (Fig. 6,  $11 \pm 9$  mM, or  $36 \pm 27\%$  resting,  $23 \pm 11$  mM, and  $6.64 \pm 0.29$  for [PCr], [Pi], and  $p\text{H}_i$ , respectively).

The presence of a remaining energy “reserve” at the limit of tolerance raises the question of what causes the exercise to be terminated. This finding is consistent with previous demonstrations and suggests that peripheral muscle “energetic failure” may not be responsible for exercise limitation (22, 49, 58). However, the regions of tissue that manifest the greatest disturbances in  $p\text{H}_i$ , [Pi], and [PCr] may also be responsible for the generation of neural feedback signals that contribute to a sense of effort and therefore exercise limitation (4). Additionally, while the reduction in [PCr] fails to explain interference with power production per se (55), it is indicative of increases in [ADP], [Pi], and  $[\text{H}^+]$  that cause muscle fatigue during high-intensity exercise through disruptions in cross-bridge cycling and  $\text{Ca}^{2+}$  handling (2). High [ADP] can disrupt power

output (9), and Pi is inversely correlated with force output (63), likely due to the disruption in myosin detachment by competitive binding of ADP and Pi to the myosin head (15, 66). Further effects on power output with high [Pi] are expected from a reduction in  $\text{Ca}^{2+}$  sensitivity at troponin C and  $\text{Ca}^{2+}$  availability by precipitate formation in the sarcoplasmic reticulum (2, 59).

While the proposed role of  $p\text{H}_i$  in mammalian skeletal muscle fatigue has been questioned (59), some reports show that it may be responsible for fatigue at, or near, physiological temperatures via alterations in  $\text{Ca}^{2+}$  sensitivity (11, 15, 50). Additionally, changes in [Pi] and  $p\text{H}_i$  both contribute to increases in the diprotonated Pi species ( $\text{H}_2\text{PO}_4^-$ ) (63), which is implicated in fatigue. Whether or not the relationship between  $[\text{H}_2\text{PO}_4^-]$  and decline in force production is causal, there is a strong correlation between muscle fatigue and  $[\text{H}_2\text{PO}_4^-]$  (8), which can, therefore, be used as an index of the potential disruption in force production. Following this logic, the distribution of  $[\text{H}_2\text{PO}_4^-]$  in the present data shows muscle regions that are expected to show a substantial reduction in peak force output at the limit of tolerance (Fig. 8) (8). This analysis suggests that peak force production in whole voxels

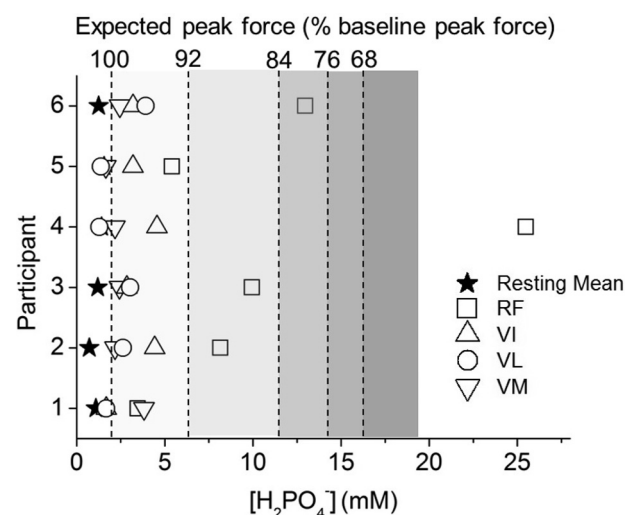


Fig. 8. Calculated concentration of diprotonated (monanionic) Pi ( $\text{H}_2\text{PO}_4^-$ ) (63) plotted for each participant at rest and at the limit of tolerance of incremental exercise in the 4 knee-extensor muscles: RF, VI, VL, VM. Symbols are as defined in Fig. 5 legend. The resting value (★) is the mean of all 4 knee extensors. Shaded panels show expected peak force as a percentage of the baseline muscle value, calculated as a function of  $\text{H}_2\text{PO}_4^-$  concentration on the basis of the relationship observed in a study of human first dorsal interosseous muscle (8).



in four of the six participants would be reduced by >10%. Whether this influence contributes to exercise limitation directly through failure of power production, or indirectly via feedback from muscle afferents, or some other process, remains to be determined. Nevertheless, while single voxels may demonstrate evidence of energetic fatigue in the present study, it appears that these regions reflect only a small proportion (<5%) of the active muscle mass.

It is currently unclear whether neural afferent feedback from stimuli arising in these regions is necessary for limiting exercise tolerance in healthy subjects. Studies using intrathecal fentanyl demonstrate that afferent feedback is vital for proper “calibration” of central motor output in healthy individuals (3–5), and that by blocking these signals it is possible to improve exercise tolerance, at least in chronic obstructive pulmonary disease (17). While the improvement in chronic obstructive pulmonary disease patient exercise tolerance was more likely from reduced ventilatory drive and reduced dyspnea, the signals generated in the periphery were presumably a driving force for a complex feedback cascade contributing to exercise limitation.

**Implications for sampling techniques.** Metabolic distributions within skeletal muscle are largely attributed to the differing enzymatic and energetic profiles of type I and II muscle fibers, and the distribution of metabolites and substrate depletion in these fibers have traditionally been investigated through biopsy. Naturally, this technique provides the advantage of direct measurement of specific cellular metabolites. Biopsy studies suggest large reductions in PCr during high-intensity cycling exercise (and accumulation of Pi, ADP, and H<sup>+</sup>) (18, 31). However, these data are of limited use in determining the responses over an entire muscle or muscle group. Biopsy volume (~50–300 mg) is typically assumed to be representative of the entire volume of muscle contributing to the exercise task [~1–3 kg per leg, based on thigh mass of ~5–7 kg in adult men (12)]. It is clear from the large variability in phosphorus metabolite concentrations reported here and elsewhere that the biopsy technique may well miss fibers that approach limiting levels or even show depletion of PCr. The biopsy technique also offers no spatial and temporal information, unless multiple sampling sites per muscle are used (raising obvious ethical and practical concerns).

Data in the literature and from our study therefore indicate that single-site sampling techniques, such as biopsy, are insufficient to characterize whole-muscle metabolism during voluntary exercise (24, 33). Based on the heterogeneity in skeletal muscle reported here and elsewhere (10, 14, 19, 24, 48), a greater spatial and temporal fidelity is needed to assess the changes in metabolic activity and fatigue-related metabolites in relation to limitation during large muscle-mass exercise.

**Conclusions.** While whole body  $\dot{V}O_2$  was linearly related to whole quadriceps [PCr] during ramp incremental exercise, the limit of tolerance was attained with a remaining intramuscular energy store and heterogeneous dynamics in all <sup>31</sup>P variables examined. The CSI technique suggests that <5% of the quadriceps muscle volume was metabolically challenged at the limit of bilateral knee extension, despite activity in the majority of the quadriceps (based on T<sub>2</sub> change) indicating the ability of these muscles to contribute power production. These data suggest that single-site sampling techniques are inadequate to characterize the heterogeneous nature of muscle metabolism

during dynamic exercise in humans. While we have used a spatially resolved technique, which substantially improves interpretation for muscle metabolite changes over unlocalized <sup>31</sup>P-MRS, Pi peak splitting was apparent in most muscle regions, indicating that further compartmentalization may mask regions of limitation. How these signals are integrated to bring about exercise intolerance in large muscle-mass exercise remains to be determined.

#### ACKNOWLEDGMENTS

We thank all study participants for their time and dedication.

#### GRANTS

This study was supported by Wellcome Trust, UK (058420 and 064898), and Biotechnology and Biological Sciences Research Council, UK (BB/100162X/1 and BB/1001174/1).

#### DISCLOSURES

No conflicts of interest, financial or otherwise, are declared by the author(s).

#### AUTHOR CONTRIBUTIONS

Author contributions: D.T.C., F.A.H., C.L., and H.B.R. analyzed data; D.T.C., F.A.H., J.R.G., and H.B.R. interpreted results of experiments; D.T.C. prepared figures; D.T.C. and H.B.R. drafted manuscript; D.T.C., F.A.H., S.A.W., D.J.M., C.L., J.R.G., G.J.K., and H.B.R. edited and revised manuscript; D.T.C., F.A.H., S.A.W., D.J.M., C.L., J.R.G., G.J.K., and H.B.R. approved final version of manuscript; F.A.H., B.J.W., S.A.W., G.J.K., and H.B.R. conception and design of research; F.A.H., B.J.W., D.J.M., and H.B.R. performed experiments.

#### REFERENCES

1. Adams GR, Duvoisin MR, Dudley GA. Magnetic resonance imaging and electromyography as indexes of muscle function. *J Appl Physiol* 73: 1578–1583, 1992.
2. Allen DG, Lamb GD, Westerblad H. Skeletal muscle fatigue: cellular mechanisms. *Physiol Rev* 88: 287–332, 2008.
3. Amann M, Blain GM, Proctor LT, Sebranek JJ, Pegelow DF, Dempsey JA. Implications of group III and IV muscle afferents for high-intensity endurance exercise performance in humans. *J Physiol* 589: 5299–5309, 2011.
4. Amann M, Dempsey JA. Locomotor muscle fatigue modifies central motor drive in healthy humans and imposes a limitation to exercise performance. *J Physiol* 586: 161–173, 2008.
5. Amann M, Proctor LT, Sebranek JJ, Pegelow DF, Dempsey JA. Opioid-mediated muscle afferents inhibit central motor drive and limit peripheral muscle fatigue development in humans. *J Physiol* 587: 271–283, 2009.
6. Beaver WL, Wasserman K, Whipp BJ. On-line computer analysis and breath-by-breath graphical display of exercise function tests. *J Appl Physiol* 34: 128–132, 1973.
7. Bottomley PA, Charles HC, Roemer PB, Flamig D, Engeseth H, Edelstein WA, Mueller OM. Human in vivo phosphate metabolite imaging with <sup>31</sup>P NMR. *Magn Reson Med* 7: 319–336, 1988.
8. Cady EB, Jones DA, Lynn J, Newham DJ. Changes in force and intracellular metabolites during fatigue of human skeletal muscle. *J Physiol* 418: 311–325, 1989.
9. Cooke R, Pate E. The effects of ADP and phosphate on the contraction of muscle fibers. *Biophys J* 48: 789–798, 1985.
10. Damon BM, Wadlington MC, Lansdown DA, Hornberger JL. Spatial heterogeneity in the muscle functional MRI signal intensity time course: effect of exercise intensity. *Magn Reson Imaging* 26: 1114–1121, 2008.
11. De Ruiter CJ, De Haan A. Temperature effect on the force/velocity relationship of the fresh and fatigued human adductor pollicis muscle. *Pflügers Arch* 440: 163–170, 2000.
12. Dempster WT. Space requirements of the seated operator: geometrical, kinematic, and mechanical aspects of the body, with special reference to the limbs. Wright-Patterson Air Force Base, OH: Wright Air Development Center US Air Force, 1955, p. 55–159.
13. Duling BR, Damon DH. An examination of the measurement of flow heterogeneity in striated muscle. *Circ Res* 60: 1–13, 1987.

14. Endo MY, Kobayakawa M, Kinugasa R, Kuno S, Akima H, Rossiter HB, Miura A, Fukuba Y. Thigh muscle activation distribution and pulmonary  $\dot{V}O_2$  kinetics during moderate, heavy, and very heavy intensity cycling exercise in humans. *Am J Physiol Regul Integr Comp Physiol* 293: R812–R820, 2007.
15. Fitts RH. The cross-bridge cycle and skeletal muscle fatigue. *J Appl Physiol* 104: 551–558, 2008.
16. Forbes SC, Slade JM, Francis RM, Meyer RA. Comparison of oxidative capacity among leg muscles in humans using gated  $^{31}\text{P}$  2-D chemical shift imaging. *NMR Biomed* 22: 1063–1071, 2009.
17. Gagnon P, Bussieres JS, Ribeiro F, Gagnon SL, Saey D, Gagne N, Provencher S, Maltais F. Influences of spinal anesthesia on exercise tolerance in patients with chronic obstructive pulmonary disease. *Am J Respir Crit Care Med* 186: 606–615, 2012.
18. Hargreaves M, McKenna MJ, Jenkins DG, Warmington SA, Li JL, Snow RJ, Febrario MA. Muscle metabolites and performance during high-intensity, intermittent exercise. *J Appl Physiol* 84: 1687–1691, 1998.
19. Houtman CJ, Heerschap A, Zwarts MJ, Stegeman DF. pH heterogeneity in tibial anterior muscle during isometric activity studied by  $^{31}\text{P}$ -NMR spectroscopy. *J Appl Physiol* 91: 191–200, 2001.
20. Iversen PO, Nicolaysen G. Local blood flow and glucose uptake within resting and exercising rabbit skeletal muscle. *Am J Physiol Heart Circ Physiol* 260: H1795–H1801, 1991.
21. Jeneson JA, Nelson SJ, Vigneron DB, Taylor JS, Murphy-Boesch J, Brown TR. Two-dimensional  $^{31}\text{P}$ -chemical shift imaging of intramuscular heterogeneity in exercising human forearm muscle. *Am J Physiol Cell Physiol* 263: C357–C364, 1992.
22. Jeneson JA, Schmitz JP, Hilbers PA, Nicolay K. An MR-compatible bicycle ergometer for in-magnet whole-body human exercise testing. *Magn Reson Med* 63: 257–261, 2010.
23. Jones NL, Killian KJ. Exercise limitation in health and disease. *N Engl J Med* 343: 632–641, 2000.
24. Kalliokoski KK, Boushel R, Langberg H, Scheede-Bergdahl C, Ryberg AK, Dossing S, Kjaer A, Kjaer M. Differential glucose uptake in quadriceps and other leg muscles during one-legged dynamic submaximal knee-extension exercise. *Front Physiol* 2: 75, 2011.
25. Kalliokoski KK, Kempainen J, Larmola K, Takala TO, Peltoniemi P, Oksanen A, Ruotsalainen U, Cobelli C, Knuuti J, Nuutila P. Muscle blood flow and flow heterogeneity during exercise studied with positron emission tomography in humans. *Eur J Appl Physiol* 83: 395–401, 2000.
26. Kalliokoski KK, Scheede-Bergdahl C, Kjaer M, Boushel R. Muscle perfusion and metabolic heterogeneity: insights from noninvasive imaging techniques. *Exerc Sport Sci Rev* 34: 164–170, 2006.
27. Kan HE, Klomp DW, Wong CS, Boer VO, Webb AG, Luijten PR, Jeneson JA. In vivo  $^{31}\text{P}$  MRS detection of an alkaline inorganic phosphate pool with short T1 in human resting skeletal muscle. *NMR Biomed* 23: 995–1000, 2010.
28. Kemp GJ, Meyerspeer M, Moser E. Absolute quantification of phosphorus metabolite concentrations in human muscle in vivo by  $^{31}\text{P}$  MRS: a quantitative review. *NMR Biomed* 20: 555–565, 2007.
29. Koga S, Poole DC, Fukuoka Y, Ferreira LF, Kondo N, Ohmae E, Barstow TJ. Methodological validation of the dynamic heterogeneity of muscle deoxygenation within the quadriceps during cycle exercise. *Am J Physiol Regul Integr Comp Physiol* 301: R534–R541, 2011.
31. Krstrup P, Soderlund K, Mohr M, Bangsbo J. The slow component of oxygen uptake during intense, sub-maximal exercise in man is associated with additional fibre recruitment. *Pflügers Arch* 447: 855–866, 2004.
32. Krstrup P, Soderlund K, Mohr M, Gonzalez-Alonso J, Bangsbo J. Recruitment of fibre types and quadriceps muscle portions during repeated, intense knee-extensor exercise in humans. *Pflügers Arch* 449: 56–65, 2004.
33. Krstrup P, Soderlund K, Relu MU, Ferguson RA, Bangsbo J. Heterogeneous recruitment of quadriceps muscle portions and fibre types during moderate intensity knee-extensor exercise: effect of thigh occlusion. *Scand J Med Sci Sports* 19: 576–584, 2009.
34. Kuschinsky W, Suda S, Sokoloff L. Local cerebral glucose utilization and blood flow during metabolic acidosis. *Am J Physiol Heart Circ Physiol* 241: H772–H777, 1981.
35. L'Abbate A, Camici P, Trivella MG, Pelosi G. Regional myocardial glucose utilization assessed by (14C) deoxyglucose. *Basic Res Cardiol* 76: 394–398, 1981.
36. Laaksonen MS, Kempainen J, Kyrolainen H, Knuuti J, Nuutila P, Kalliokoski KK. Regional differences in blood flow, glucose uptake and fatty acid uptake within quadriceps femoris muscle during dynamic knee-extension exercise. *Eur J Appl Physiol* 113: 1775–1782, 2013.
37. Meyer RA. Linear dependence of muscle phosphocreatine kinetics on total creatine content. *Am J Physiol Cell Physiol* 257: C1149–C1157, 1989.
38. Meyer RA, Prior BM. Functional magnetic resonance imaging of muscle. *Exerc Sport Sci Rev* 28: 89–92, 2000.
39. Mizuno M, Kimura Y, Iwakawa T, Oda K, Ishii K, Ishiwata K, Nakamura Y, Muraoka I. Regional differences in blood flow and oxygen consumption in resting muscle and their relationship during recovery from exhaustive exercise. *J Appl Physiol* 95: 2204–2210, 2003.
40. Moon RB, Richards JH. Determination of intracellular pH by  $^{31}\text{P}$  magnetic resonance. *J Biol Chem* 248: 7276–7278, 1973.
41. Morikawa S, Inubushi T, Kito K, Tabata R. Imaging of phosphoenergetic state and intracellular pH in human calf muscles after exercise by  $^{31}\text{P}$  NMR spectroscopy. *Magn Reson Imaging* 12: 1121–1126, 1994.
42. Myers J, Prakash M, Froelicher V, Do D, Partington S, Atwood JE. Exercise capacity and mortality among men referred for exercise testing. *N Engl J Med* 346: 793–801, 2002.
43. Naressi A, Couturier C, Devos JM, Janssen M, Mangeat C, de Beer R, Graveron-Demilly D. Java-based graphical user interface for the MRUI quantitation package. *MAGMA* 12: 141–152, 2001.
44. Nelson SJ, Taylor JS, Vigneron DB, Murphy-Boesch J, Brown TR. Metabolite images of the human arm: changes in spatial and temporal distribution of high energy phosphates during exercise. *NMR Biomed* 4: 268–273, 1991.
45. Pesta D, Paschke V, Hoppel F, Kobel C, Kremser C, Esterhammer R, Burtscher M, Kemp GJ, Schocke M. Different metabolic responses during incremental exercise assessed by localized  $^{31}\text{P}$  MRS in sprint and endurance athletes and untrained individuals. *Int J Sports Med*. In press.
46. Piiper J. Perfusion, diffusion and their heterogeneities limiting blood-tissue  $O_2$  transfer in muscle. *Acta Physiol Scand* 168: 603–607, 2000.
47. Piiper J, Haab P. Oxygen supply and uptake in tissue models with unequal distribution of blood flow and shunt. *Respir Physiol* 84: 261–271, 1991.
48. Richardson RS, Haseler LJ, Nygren AT, Bluml S, Frank LR. Local perfusion and metabolic demand during exercise: a noninvasive MRI method of assessment. *J Appl Physiol* 91: 1845–1853, 2001.
49. Rodenburg JB, de Boer RW, Jeneson JA, van Echteld CJ, Bar PR.  $^{31}\text{P}$ -MRS and simultaneous quantification of dynamic human quadriceps exercise in a whole body MR scanner. *J Appl Physiol* 77: 1021–1029, 1994.
50. Roots H, Ball G, Talbot-Ponsonby J, King M, McBeath K, Ranatunga KW. Muscle fatigue examined at different temperatures in experiments on intact mammalian (rat) muscle fibers. *J Appl Physiol* 106: 378–384, 2009.
51. Rossiter HB, Howe FA, Ward SA. Intramuscular phosphate and pulmonary  $\dot{V}O_2$  kinetics during exercise. In: *Oxygen Uptake Kinetics in Sport, Exercise, and Medicine*, edited by Jones AM and Poole DC. London: Routledge, 2005, p. 154–184.
52. Rossiter HB, Ward SA, Doyle VL, Howe FA, Griffiths JR, Whipp BJ. Inferences from pulmonary  $O_2$  uptake with respect to intramuscular [phosphocreatine] kinetics during moderate exercise in humans. *J Physiol* 518: 921–932, 1999.
53. Rossiter HB, Ward SA, Howe FA, Kowalchuk JM, Griffiths JR, Whipp BJ. Dynamics of intramuscular  $^{31}\text{P}$ -MRS Pi peak splitting and the slow components of PCr and  $O_2$  uptake during exercise. *J Appl Physiol* 93: 2059–2069, 2002.
54. Rossiter HB, Ward SA, Howe FA, Wood DM, Kowalchuk JM, Griffiths JR, Whipp BJ. Effects of dichloroacetate on  $\dot{V}O_2$  and intramuscular  $^{31}\text{P}$  metabolite kinetics during high-intensity exercise in humans. *J Appl Physiol* 95: 1105–1115, 2003.
55. Sahlin K, Soderlund K, Tonkonogi M, Hirakoba K. Phosphocreatine content in single fibers of human muscle after sustained submaximal exercise. *Am J Physiol Cell Physiol* 273: C172–C178, 1997.
56. van Laar PJ, van der Grond J, Hendrikse J. Brain perfusion territory imaging: methods and clinical applications of selective arterial spin-labeling MR imaging. *Radiology* 246: 354–364, 2008.
57. Vandeborne K, Walter G, Leigh JS, Goelman G. pH heterogeneity during exercise in localized spectra from single human muscles. *Am J Physiol Cell Physiol* 265: C1332–C1339, 1993.

58. **Vanhatalo A, Fulford J, DiMenna FJ, Jones AM.** Influence of hyperoxia on muscle metabolic responses and the power-duration relationship during severe-intensity exercise in humans: a  $^{31}\text{P}$  magnetic resonance spectroscopy study. *Exp Physiol* 95: 528–540, 2010.
59. **Westerblad H, Allen DG, Lannergren J.** Muscle fatigue: lactic acid or inorganic phosphate the major cause? *News Physiol Sci* 17: 17–21, 2002.
60. **Whipp BJ, Davis JA, Torres F, Wasserman K.** A test to determine parameters of aerobic function during exercise. *J Appl Physiol* 50: 217–221, 1981.
61. **Whipp BJ, Rossiter HB, Ward SA.** Exertional oxygen uptake kinetics: a stamen of stamina? *Biochem Soc Trans* 30: 237–247, 2002.
62. **Whipp BJ, Rossiter HB, Ward SA, Avery D, Doyle VL, Howe FA, Griffiths JR.** Simultaneous determination of muscle  $^{31}\text{P}$  and  $\text{O}_2$  uptake kinetics during whole body NMR spectroscopy. *J Appl Physiol* 86: 742–747, 1999.
63. **Wilson JR, McCully KK, Mancini DM, Boden B, Chance B.** Relationship of muscular fatigue to pH and diprotonated Pi in humans: a  $^{31}\text{P}$ -NMR study. *J Appl Physiol* 64: 2333–2339, 1988.
64. **Wray DW, Nishiyama SK, Monnet A, Wary C, Duteil S, Carlier PG, Richardson RS.** Multiparametric NMR-based assessment of skeletal muscle perfusion and metabolism during exercise in elderly persons: preliminary findings. *J Gerontol A Biol Sci Med Sci* 64: 968–974, 2009.
65. **Wray DW, Nishiyama SK, Monnet A, Wary C, Duteil SS, Carlier PG, Richardson RS.** Antioxidants and aging: NMR-based evidence of improved skeletal muscle perfusion and energetics. *Am J Physiol Heart Circ Physiol* 297: H1870–H1875, 2009.
66. **Yamashita H, Sata M, Sugiura S, Momomura S, Serizawa T, Iizuka M.** ADP inhibits the sliding velocity of fluorescent actin filaments on cardiac and skeletal myosins. *Circ Res* 74: 1027–1033, 1994.

